https://doi.org/10.5194/nhess-2023-39
Preprint. Discussion started: 28 March 2023

Natural Hazards and Earth System Sciences
Discussions

The climatology and nature of warm-season convective cells in cold-frontal environments over Germany

George Pacey[1], Stephan Pfahl[1], Lisa Schielicke[1,2], and Kathrin Wapler[3]

[1]Institute of Meteorology, Freie Unversität Berlin, Berlin, Germany
[2]Department of Meteorology, University of Bonn, Bonn, Germany
[3]Deutscher Wetterdienst, Offenbach, Germany

Correspondence: George Pacey (george.pacey@fu-berlin.de)

Abstract. Cold fronts provide an environment particularly favourable for convective initiation in the mid-latitudes and can also be associated with convective hazards such as wind, rain and hail. We build a climatology of cold-frontal convective cells between 2007–2016 for April–September in a cell-front distance framework by combining a radar-based cell detection and tracking dataset and automatic front detection methods applied to reanalysis data. We find that on average around twice as many cells develop on cold-frontal cell days compared to non-cold-frontal cell days. Using the 700 hPa level as a reference point we show the maximum cell frequency is 350–400 km ahead of the 700 hPa front which is marginally ahead of the mean surface front location. The 700 hPa front location marks the minimum cell frequency and a clear shift in regime between cells with a weakened diurnal cycle on the warm-side of the 700 hPa cold front and strongly diurnally driven cells on the cold-side of the 700 hPa front. High cell frequencies are found several hundreds of kilometres ahead of the surface front and cells in this region are most likely to be associated with mesocyclones, intense convective cores and lightning. These results are an important step towards a better understanding of cold-frontal convection climatology and links between cold fronts and convective hazards.

1 Introduction

Atmospheric convection is a key process in the formation of certain atmospheric hazards such as extreme precipitation, hail and lightning. In Europe, convective loss events to the insurance industry have risen by around a factor of 4 from about 30 events per year in 1980 to about 120 in 2014 (Hoeppe, 2016). Germany is particularly prone to such convective loss events with some events leading to insurance losses of over 1 billion euros (Kunz et al., 2018 and Wilhelm et al., 2021). Taszarek et al. (2019) showed based on European Severe Weather Database reports (ESWD; Dotzek et al., 2009) that much of Germany reports 8 or more days per year with heavy convective precipitation (their Figure 7). Recent events such as the exceptional floods of Central Europe in July 2021 (Mohr et al., 2023), which was exacerbated by embedded convection, highlight the need for further information on the underlying processes that lead to heavy convective precipitation.

Deep moist convection (DMC) frequently initiates in proximity to air mass boundaries such as synoptic-scale fronts (length scale of ~1000 km), drylines and outflow boundaries (Markowski and Richardson, 2010). While cold-frontal convection is frequent during the warm-season, convection rarely initiates along the entirety of the boundary. This indicates that the precise

https://doi.org/10.5194/nhess-2023-39
Preprint. Discussion started: 28 March 2023


Natural Hazards and Earth System Sciences Discussions

location of convective initiation is likely due to underlying mesoscale processes (Markowski and Richardson, 2010). Such processes are not currently well-understood, thus forecasting of cold-frontal convection is challenging. Previous studies including field experiments (e.g., Wulfmeyer et al., 2011, Bott, 2012 and Lee et al., 2016) have demonstrated that fronts can favour the occurrence of convection due to different mechanisms depending on the convective initiation location. The pre-frontal environment is the region ahead of a cold front, which typically corresponds to the warm sector of extratropical cyclones. Convection can be triggered by the convergence of warm and humid air masses near the surface; for example, near the surface front or at pre-surface-frontal convergence lines (e.g., Wulfmeyer et al., 2011 and Dahl and Fischer, 2016). The high temperatures and moisture content pre-frontal also contribute to atmospheric instability. The ageostrophic frontal circulation which leads to lifting (Bluestein, 1993) can also help air parcels overcome convective inhibition (CIN). Convection may also be embedded in stratiform rain regions, sometimes in the form of narrow cold-frontal rainbands (Gatzen, 2011 and Clark, 2013). These mostly occur in the cool-season and thus will not be explicitly addressed in this study. Convection may also initiate behind a cold front in the post-frontal environment mainly due to the destabilisation of the air masses associated with the transport of colder air over a potentially warmer surface (Weusthoff and Hauf, 2008 and Bott, 2012). Convection can occur simultaneously pre-frontal, frontal and post-frontal depending on environmental conditions (Ferretti et al. 2014).

Due to the sloped nature of cold fronts there is no concrete and uniform definition of post-frontal, frontal and pre-frontal convection in the literature. Some studies consider any convection behind the surface cold front to be post-frontal, including convection embedded in the frontal rainband (e.g., Schumacher et al., 2022). As a surface observer this holds true, but the saturated cloud region and thus any embedded convection is likely located on the warm-side of the cold front. Other studies consider post-frontal convection to be the diurnally driven mostly surface-based convection that is typically seen in the form of isolated showers or thunderstorms (e.g., Weusthoff and Hauf, 2008 and Bott, 2012). Likewise, it is not clear at which point the transition from post-frontal to frontal or frontal to pre-frontal should be. With this in mind we produce a cold-frontal convective cell climatology largely in a cell-front distance framework.

Previous studies relating to cold fronts and convection in Europe have primarily focused on narrow cold-frontal rainbands (Gatzen, 2011 and Clark, 2013). In addition, Schemm et al. (2016) showed up to 45% of all detected hail events in north-eastern and southern Switzerland form in pre-frontal zones arguing that vertical wind shear and along frontal moisture transport were among the mechanisms favouring hail formation in pre-frontal environments. Kunz et al. (2020) found frontal convective storms associated with hail produce larger hailstones and have longer tracks on average and that a front was needed to trigger 50% of severe convective storms over flat-terrain in Germany.

In this study we focus on warm-season cold-frontal convection (April–September) and use a broader definition of convection which is based on radar reflectivity and area thresholds thus is not solely based on convective lines (as in Gatzen, 2011 and Clark, 2013). We seek to shed light on the climatology and nature of convective cells in cold-frontal environments over Germany in a comprehensive framework, that is to say, considering the cell climatology and attributes depending on the distance from the front. To our knowledge, a study incorporating such aspects is not present in current literature. We also seek to highlight the differences between cold-frontal convective cells and non-cold-frontal convective cells. The primary research questions addressed in this study are as follows:

https://doi.org/10.5194/nhess-2023-39
Preprint. Discussion started: 28 March 2023


Natural Hazards and Earth System Sciences
Discussions

Q1) How do the spatial and temporal frequency of convective cells differ depending on the cell's distance from the front?
Q2) How does the nature of convective cells differ depending on the cell's distance from the front?
Q3) How do Q1 and Q2 compare to non-cold-frontal convective cells?

The paper is organised as follows: Section 2 will introduce the convective cell detection and tracking dataset as well as the automatic front detection methods that are applied to ERA5 reanalysis data. We also show front detection examples for cases with convective cells in proximity. Section 3 will highlight the key results of the study and put them in the context of the current literature. The subsections focus on convective cell count and cell days, diurnal cycle, spatial climatology and the nature of convective cells. For the nature of cells we investigate cell lifetime, propagation speed, organisation, lightning frequency, intensity, and mesocyclone frequency. In Section 4 we summarise the results and highlight the importance of this work.

2 Data and Methods

We combine two datasets: ERA5 reanalysis data (Hersbach et al., 2018, 2020) and the KONRAD Convective Cell Detection and Tracking Dataset (Wapler and James, 2014). Automatic front detection methods are applied to the ERA5 reanalysis dataset (Section 2.1) and KONRAD (Section 2.2) is used for the convective cell definitions. ERA5 is available between 1959 to present whereas KONRAD was available from 2007–2016 for the months April–September, thus we use the KONRAD availability period for our analysis. The spatial and temporal resolutions of ERA5 are 1 hour and 0.25 degrees and 5 minutes and 1 km for KONRAD.

2.1 Front Detection

A front is generally considered a boundary between air masses with different properties such as temperature and humidity. Forecasters are primarily interested in synoptic-scale fronts as they are the main driver of precipitation in the mid-latitudes (Catto and Pfahl, 2013). Forecasters often manually position such fronts based on numerical weather prediction (NWP) output and observations. They sometimes use more technical algorithms. However, as noted by Renard and Clarke (1965), different forecasters produce different analyses thus the final front location can be subjective depending on the forecaster. An additional problem is that archives of such analyses are sparse in both space and time. Renard and Clarke (1965) was one of the first studies that recognised the need for objective methods to detect fronts, and since then, automatic front detection in reanalysis data has attracted increasing attention (e.g., Hewson, 1998; Jenkner et al., 2010; Schemm et al., 2015, 2016, 2018; Thomas and Schultz, 2019 and Rüdisühli et al., 2020). All of these studies reference the Thermal Front Parameter equation (Equation 1) which was first introduced by Renard and Clarke (1965).

$$\mathrm{TFP} = -\nabla|\nabla\tau| \cdot \frac{\nabla\tau}{|\nabla\tau|} \tag{1}$$

https://doi.org/10.5194/nhess-2023-39
Preprint. Discussion started: 28 March 2023


Natural Hazards and Earth System Sciences
Discussions

The term represents the rate of change of τ projected in the direction of the thermal gradient, where τ is a thermodynamic variable (e.g., potential temperature or equivalent potential temperature). The projection takes the curvature of fronts into account. Since the term is a double derivative an inflexion point is found where the parameter is equal to zero corresponding to the maximum in the thermal gradient. The horizontal wind (**v**) can be projected onto the frontal line using Equation 2 (Hewson, 1998).

$$v_f = \mathbf{v} \cdot \frac{\nabla(\mathrm{TFP})}{|\nabla(\mathrm{TFP})|} \tag{2}$$

The term v_f is the horizontal wind (**v**) projected in the direction of the TFP gradient. It is positive at cold fronts and negative at warm fronts. The v_f threshold can be altered to consider fronts meeting a minimum advection criteria. Higher values of v_f indicate stronger advection at the frontal boundary. Stationary fronts are found where $v_f \approx 0$.

2.1.1 Criteria

In this study, the cold-frontal regions are detected using the following criteria:

$$|\nabla\theta_e| > 6\,\mathrm{K}(100\,\mathrm{km})^{-1} \tag{3}$$

$$v_f > 1\,\mathrm{ms}^{-1} \tag{4}$$

$$L > 1000\,\mathrm{km} \tag{5}$$

The equivalent potential temperature is represented by θ_e and is used as the thermodynamic variable τ. The along front length is represented by L. The overlap of the θ_e gradient threshold (3) and velocity threshold (4) represents the front contour. Since we are only interested in synoptic fronts (~1000 km), fronts with an along front length (L) less than 1000 km are omitted from the analysis. The frontal line is identified at the maximum of the equivalent potential temperature gradient by applying the following condition:

$$\mathrm{TFP} = 0 \tag{6}$$

These four criteria are applied to smoothed θ_e and horizontal wind fields at 700 hPa in the ERA5 reanalysis data. The fields are smoothed 30 times using a simple smoothing function whereby the nearest four neighbours of a grid point are averaged and the process is repeated 30 times in order to remove any local-scale features. We use the same temperature gradient threshold and height level as applied in Schemm et al. (2016) who focused on cold fronts and hail in Switzerland. The pressure level chosen is to avoid inference with orography, which is particularly an issue in central Europe (Jenkner et al., 2010, their section 4.4). Furthermore, the 700 hPa level is further from the turbulent boundary layer. We recognise the 700 hPa level is not the typical height level used by forecasters to identify fronts, but due to the complexities of automatic front detection it is important to derive smooth frontal lines for the cell-front distance calculations and limit the number of erroneously detected fronts. Equivalent potential temperature is selected over potential temperature since it is a function of both temperature and moisture thus gives the strongest frontal signal. One disadvantage to θ_e is that temperature and humidity can vary independently thus

https://doi.org/10.5194/nhess-2023-39
Preprint. Discussion started: 28 March 2023


Natural Hazards and Earth System Sciences Discussions

localised humidity gradients could be detected (as discussed in Thomas and Schultz, 2019). However, due to the strict 1000 km length threshold and smoothing filter such smaller-scale fronts such as sea-breeze, land-breeze and gust fronts will be largely filtered out. Therefore, further filtering of local and synoptic fronts, as carried out by Jenkner et al. (2010) and Rüdisühli et al. (2020) for convective-permitting datasets, is not required. The velocity threshold incorporates near-stationary to fast moving cold fronts.

The thresholds chosen (3), (4), (5) are stricter than some previous studies. Lower thresholds would increase the number of erroneously detected fronts while higher thresholds generally reduce the number of fronts in the dataset but limit the dataset to synoptic-scale cold fronts only. We value a dataset with a lower front count and higher percentage of correctly detected fronts. Cold fronts are detected in a subsection of the European domain ([40N–70N, 20W–20E], see Figure 1).

2.1.2 Validation

Validation was carried out by manually viewing one year of data and several other case studies to verify that frontal features resembled synoptic-scale fronts (see examples in Figure 2). Figure 1 shows a spatial map with the number of cold-frontal days per warm season between 2007–2016 for April–September to verify plausible spatial distributions. The highest cold-frontal day frequency is over the southern half of the United Kingdom, northern France, the Low Countries and north-western Germany totalling between 20–23 front days per warm season. The minimum is found in the south-east of the domain. However, there is a slight sample bias for grid points at the edge of the domain since fronts extending beyond the domain may not always meet the 1000 km length criterion. Fronts typically decay as they experience friction from the surface over land. The cold-frontal day maximum is located close to the edge of continental Europe which could be explained by slowly propagating fronts being detected across several days. A boundary is also evident around the Alps which is likely linked to cold fronts becoming distorted and weakening when interacting with orography (Schumann, 1987). This boundary can also be identified in Kunz et al. (2020)'s cold front climatology between 2005–2014 (their Figure 3).

2.2 KONRAD Convective Cell Detection and Tracking Algorithm

KONRAD (KONvektionsentwicklung in RADarprodukten, convection evolution in radar products) is a convective cell detection and tracking algorithm originally applied to 2D radar data in the German radar domain (see Figure 2) (Wapler and James, 2014). At the start of this study KONRAD3D (Werner, 2017) was in the final stages of development and was not available over a long time-series so we used the original KONRAD based on 2D radar data. KONRAD is run operationally by the German Weather Service (DWD) with a spatial and time resolution of 1 km and 5 minutes, respectively. A convective cell is defined as one with 15 pixels or more exceeding 46 dBZ. Since the resolution of KONRAD is 1 km, 1 pixel ~ 1 km^2. The reflectivity is based on a 0.5 degree radar scan thus the height relative to the ground varies with distance from the radar and due to orography. Where two radar scans overlap the highest dBZ value is used. KONRAD also provides a parameter which indicates the likelihood of hail (the hail flag) ranging from 0 to 2. The parameter is based on cell intensity and area thresholds. A hail flag value of 1 is assigned if at least one pixel in the cell exceeds 55 dBZ. A hail flag value of 2 is assigned if 12 or more pixels exceed 55 dBZ or if at least one pixel exceeds 60 dBZ. Otherwise a hail flag of 0 is assigned. Additional information in

https://doi.org/10.5194/nhess-2023-39
Preprint. Discussion started: 28 March 2023


Natural Hazards and Earth System Sciences Discussions

relation to the detected convective cells has been made available such as the number of lightning strikes in proximity to the cell centre and mesocyclone characteristics. The lightning strike data are based on the time of arrival method from the European VLF/LF LIghtning detection NETwork (LINET, Betz et al., 2009). A mesocyclone detection algorithm is run operationally by the DWD using doppler radar data (Hengstebeck et al., 2018). The severity of mesocyclones is given a ranking from 1 to 5. We include mesocyclones of ranking 3 or higher in order to include a sample with significant size and mesocyclone strength. To be classified as a mesocyclone with severity level 3 the following criteria must be met: 5 km equivalent diameter, 3 km depth, 10^{-3} s^{-1} azimuthal shear or 15 ms^{-1} rotational velocity. A detailed description of the algorithm and practical examples can be found in Hengstebeck et al. (2018). Such information will be utilised in section 3.4. However, for all other sections the convective cell definition is based on 15 pixels or more exceeding 46 dBZ. This definition includes cells of moderate to severe intensity. Excluding section 3.4, we consider cells at their first detection time only to avoid repeat counting at additional timesteps in the climatology.

2.3 Cell and front detection examples

Combining the methods introduced in Section 2.1 and 2.2 four cases are shown in Figure 2 for single timesteps. The cold-frontal line (blue contour) is the result of applying the conditions (3), (4), (5) and (6). Convective cells are considered to be associated to a front in the hour following the front detection. For example, for a front detection at 13 UTC, cells that were first detected between 13:00–13:59 UTC are included. The distance between the convective cell and the 700 hPa frontal line (hereafter cell-front distance) is the distance between the convective cell centre and the nearest grid point on the 700 hPa frontal line contour (i.e. the shortest distance between the frontal line and the convective cell on the surface of an ellipsoidal model of the earth; Karney, 2013). A cell is assigned a positive distance if the average θ_e surrounding the cell location (4 grid points) is equal to or greater than the frontal line θ_e, thus indicating the cell is on the warm-side of the 700 hPa front. Otherwise, the cell is assigned a negative distance indicating the cell is on the cold-side of the 700 hPa front. Timesteps containing two or more cold-frontal lines in the domain [40N–70N,5W–20W] were omitted due to uncertainly on deriving the cell-front distance. This resulted in 3,506 (18.8%) of the total 18,613 frontal timesteps being omitted. In the examples (Figure 2) we highlight situations with cells on the warm-side of the 700 hPa front (hereafter pre-700-frontal), in close proximity to the 700 hPa front (near-700-frontal) and also behind the 700 hPa front (post-700-frontal). In some cases they occur simultaneously in the KONRAD domain (black contour). A NE-SW oriented front is located over Germany in In Figure 2a with pre-700-frontal convective cells. A line of cells can be found between 250–400 km ahead of the 700 hPa front. The second case (Figure 2b) shows a cold front that has progressed across Germany and is located in proximity to the Alps. Cells are located post-700-frontal between 350–750 km from the 700 hPa front. Like Figure 2a, Figure 2c also shows a pre-700-frontal case study but with a front oriented more towards the N-S direction and with more curvature. A larger number of cells are associated with this case with cells in a larger range of distances between ~100–750 km ahead of the 700 hPa frontal line. The final example (Figure 2d) shows a front oriented NE-SW through the middle of the radar domain. Cells are located both pre-700-frontal and post-700-frontal.

https://doi.org/10.5194/nhess-2023-39
Preprint. Discussion started: 28 March 2023


Natural Hazards and Earth System Sciences Discussions

3 Results

3.1 Convective cell count and days

During the period 2007–2016 for the months April–September 258,218 cells were detected in KONRAD (Section 2.2). These cells were detected on 1389 warm-season days out of a possible 1830, thus cells develop on 76% of warm-season days in Germany. On cold-frontal cell days, 163,255 cells (63%) were detected. A cold-frontal cell day is defined as one where at least one convective cell was detected within 750 km of the 700 hPa frontal line. The remaining 94,963 (37%) cells were detected on non-cold-frontal days. A cell was found to be associated to a cold front on 614 days, thus approximately a third of warm-season days are associated with cold-frontal convection in Germany. We remark that this does not imply a new frontal system every 3 days as many cases are associated with slowly propagating fronts across several days. While a slightly larger percentage of all cell days were non-cold-frontal cell days (56%), over twice as many cells developed on average on cold-frontal cell days (266 cells per day) compared to non-cold-frontal cell days (123 cells per day) (Figure 3). The 95th percentile of the cells per day is 725 accounting for 80 days. 80% of these days occurred on cold-frontal cell days. This highlights that extreme events (in terms of cell count per day) are significantly more likely on cold-frontal cell days. The differences in the cell per day count could reflect convection being more widespread across Germany and/or more cells associated to each cell cluster. These results are consistent with findings from Wapler and James (2014) who found the synoptic patterns with the highest number of convective cells were Cyclonic Southerly, Anticyclonic South-Easterly, Cyclonic South- Westerly and Trough over Western Europe. All of which are likely to indicate the presence of a cold front excluding Anticyclonic South-Easterly. The cell statistics are summarised in Table 1.

Figure 4 illustrates the number of convective cells (blue) and the number of convective cell days (red) depending on the cell-front distance. The number of convective cell days refers to the number of days a cell was found between each 50 km interval shown in Figure 4. Positive distances indicate pre-700-frontal cells and negative distances post-700-frontal cells. A total of 65,567 cells were found in proximity ($\pm$750 km) to the 700 hPa frontal line between 2007–2016 (April–September). The 65,567 cells are a subset of the 163,255 cells on cold-frontal cell days, the remaining cells occurred outside of the 750 km range, on timesteps with 2 or more fronts or on timesteps with no cold front detected. The most common region for cells is pre-700-frontal accounting for 84% of all cells. The maximum is 350–400 km ahead of the 700 hPa front. This corresponds to the location marginally ahead of the mean surface front location, assuming the 700 hPa level is found ~3000 metres above the surface and the cold front has a slope of ~1:100. This assumption was supported by an analysis in ERA5 data which showed the climatological maximum of surface convergence is 300 km ahead of the 700 hPa front (not shown). Whilst the slope of the front and corresponding surface front location is likely to vary slightly per case study we proceed assuming the climatological location of the surface front is 300 km ahead of the 700 hPa frontal line. Behind the surface front the cell frequency steeply declines towards the 700 hPa front. The 700 hPa frontal line corresponds to the minimum cell frequency. This also justifies our use of the 700 hPa level since it marks a clear shift in the probability of convective cells. This minimum could be linked to the descent observed behind a cold front (Davies and Wernli, 2015). Synoptic-scale fronts are typically analysed by forecasters at the surface or 850 hPa, thus forecasters should not expect the lowest chance of cells to be after the front has passed at 850

https://doi.org/10.5194/nhess-2023-39
Preprint. Discussion started: 28 March 2023


Natural Hazards and Earth System Sciences Discussions

hPa or the surface, rather after the frontal passage at 700 hPa. Cells in the post-700-frontal environment account for 16% of all cells. Similar to the pre-700-frontal environment, there is a relatively normalised distribution around the maximum frequency 350–400 km behind the front. Assuming post-700-frontal convection is primarily driven by solar heating, a certain period is likely required after the front passes before convective initiation is favourable.

The number of convective cell days is shown in Figure 4b showing a similar distribution as the total number of cells with a slight shift in the maximum further from the 700 hPa front. This is true both post-700-frontal and pre-700-frontal with the new maximum found -500 to -450 km and 400 to 450 km from the 700 hPa front respectively. While approximately 5 times as many cells were found around the pre-700-frontal maximum (~5000 cells) compared to the post-frontal maximum (~1000 cells, see Figure 4a), the number of cell days differs by a factor of 2.5. Therefore, pre-700-frontal cases are associated with a greater number of cells than post-700-frontal cases which explains the significant difference in the magnitude of the peak when looking at the total number of cells. Since cold fronts typically decay as they move over continental Europe there is a possible sample bias with more pre-700-frontal environments being sampled than post-700-frontal environments. This bias was assessed by counting the total available timesteps at each distance relative to the front. This showed that the pre-700-frontal environment was sampled between 20–30% more often than the post-700-frontal environment. However, when plotting the percentage of total available timesteps with cells an identical distribution was found as in Figure 4a.

3.2 Diurnal Cycle

Convection is known to generally exhibit a diurnal cycle with a maximum in the afternoon hours and a minimum in the early morning hours (Ban et al., 2014). The number of cells is shown as a function of the cell-front distance and hour of the day in Figure 5. Firstly, as noted in Figure 4, the maximum cell count is found in the pre-700-frontal environment with the minimum surrounding the 700 hPa front. Figure 5 highlights that most post-700-frontal cells develop during the daytime hours (especially between 10–18 UTC) with low cell frequency outside of this period. In contrast, pre-700-frontal cells do develop in the night hours and the cell maximum is shifted later in the day. The exception to this is further from the front in the region 750–1000 km where cells have a stronger diurnal cycle. We speculate that the lifting associated with the front is weaker this far from the front thus cells are largely diurnally driven. This result also justifies our distance criterion at which we consider a convective cell to be associated to a front, that is, within 750 km of the 700 hPa frontal line.

Figure 6 shows the same data as Figure 5 but with an average taken across the pre-700-frontal (0 to 750 km) and post-700-frontal (-750 to 0 km) environments. The diurnal cycle of non-cold-frontal cells (green) is shown for reference. A strong diurnal cycle for post-700-frontal cells (blue line) is evident with a maximum between 15–16 UTC. The distribution for non-cold-frontal cells is similar with a maximum also between 15–16 UTC. The pre-700-frontal maximum is found between 16–17 UTC, a later peak than in the non-cold-frontal and post-700-frontal categories. The weakened cycle is evident by the larger percentage of cells occurring during the night-time hours. Between 21–06 UTC, 31% of pre-700-frontal cells developed compared to only 9% and 13% of post-700-frontal and non-cold-frontal cells respectively. A similar weakening of the diurnal cycle was observed for mesocyclones compared to lightning in Germany (Wapler et al., 2016). Furthermore, Morel and Senesi (2002) found that mesoscale convective systems (MCSs) dissipate most commonly at 21 Local Solar Time (LST) on average in

https://doi.org/10.5194/nhess-2023-39
Preprint. Discussion started: 28 March 2023


Natural Hazards and Earth System Sciences Discussions

Europe. Surowiecki and Taszarek (2020) found a similar result showing the majority of MCSs dissipate around 19–20UTC in Poland, though squall line/bow echo MCSs most frequently dissipate at midnight. MCSs typically live longer than individual cells, and new cells may be triggered throughout their lifecycle, e.g. through interaction with the cold pool/convective outflow which is less dependant on solar forcing. We speculate therefore that the observed pre-700-frontal weakened diurnal cycle could be linked to mesoscale convective systems. We also investigated the monthly cycle of convective cells depending on the cell-front distance but no significant differences were found with the peak season being mid-July. The peak season for non-cold-frontal cells was early July.

3.3 Spatial cell climatology

The spatial frequency of convective events in Europe has been shown to vary (Groenemeijer et al., 2017; Taszarek et al., 2019 and 2020). Schemm et al. (2016) also showed the fraction of hail events associated with a synoptic-scale cold front varied spatially across Switzerland and the vicinity. In this section we produce spatial maps of convective cell days per warm season in the KONRAD radar domain (shown by the grey contour in Figure 7). As in Figure 3, a cell day is defined as one where at least one convective cell was detected, in this case within a 1 x 1 degree grid box.

3.3.1 Convective cell days

Distinct spatial distributions were found for pre-700-frontal and post-700-frontal cells (Figure 7). Post-700-frontal cells (Figure 7a) are most frequent in north-west Germany developing between 5–8 days per warm season. The highest frequency is near the coastline, possibly due to multiple factors such as sea-breezes, higher moisture availability and increased lift with cooler air being advected over a warmer surface. Moving south and east the number of cells per warm season reduces to 1–3. Pre-700-frontal cells (Figure 7b) are most frequent in the southern half of Germany, particularly in the far south near the borders with France, Switzerland and Austria. Cells develop between 8–16 days per warm season in the majority of the domain in the pre-700-frontal environment. The exceptions are grid boxes outside of Germany which are likely under-sampled as they are located further from radars (see bounds in grey). The combined pre-700-frontal and post-700-frontal convective cell spatial distribution shows one maximum in southern Germany and another in north-west Germany (Figure 7c). North-east Germany receives the lowest number of cold-frontal cell days per warm season. The non-cold-frontal (Figure 7d) and all cells spatial distributions (Figure 7e) are very similar to pre-700-frontal cells (Figure 7b).

3.3.2 Cold-frontal cell day fraction

Figure 7f shows the percentage of all convective cell days associated with cold fronts for 1 x 1 degree grid boxes. Around 35–40% of convective cell days were associated with cold fronts for much of north-western Germany. The percentage decreases moving further south and east. In south-eastern and eastern Germany, the western Czech Republic and western Poland only 20–30% of cell days were cold-frontal. Kunz et al. (2020) showed that over complex terrains, the proportion of frontal severe

https://doi.org/10.5194/nhess-2023-39
Preprint. Discussion started: 28 March 2023


Natural Hazards and Earth System Sciences
Discussions

convective storms is around 10–15%, while over flat terrain 50% require a frontal trigger. In our analysis, we find a similar result with the lowest frontal fraction in southern Germany (Alps) and near the mountainous German-Czech border.

3.3.3 Cold front types

The orientation and geographic location of cold fronts could potentially be used as an indicator for the likelihood of cells. To investigate this, 4,230 frontal timesteps with convective cells were clustered into 30 clusters using k-means clustering (section 14.3.1 in Wilks, 2006) such that each cluster contains fronts with similar characteristics (i.e, spatially located and orientated in a similar way). A cropped domain ([40N–60N,0–20E]) of the original front detection domain (Figure 1) was used. K-means is an unsupervised machine learning algorithm which requires the number of clusters to be predefined. Cluster numbers between 10 and 50 were tested to find the optimum cluster number in terms of not too many clusters resulting in large similarities between clusters but not too little resulting in fronts with different features being grouped in the same cluster. The final cluster number of 30 was chosen subjectively based on these criteria and 6 clusters (1,133 timesteps) were removed due to a lack of continuity in the clusters. We draw frontal contours (Figure 8) where 50% of timesteps in the respective cluster had the front located at that grid point.

The resulting 24 front clusters are shown in Figure 8 sorted by the overall largest number of convective cells per timestep. The colourbar represents the number of cells per timestep per 1 x 1 degree grid box. Cluster 1 has the highest cell frequency which is associated with a NE-SW oriented front extending from Scandinavia to France. The highest cell frequency is in the western half of Germany located ahead of the 700 hPa frontal location, consistent with our results shown in Figure 4. The convective cell minimum around the 700 hPa frontal location can also be located in several clusters (e.g., Clusters 11, 15 and 20). Cluster 2 and 3 show similar front types to Cluster 1 but are positioned slightly further west (Cluster 2) or east (Cluster 3). Post-700-frontal cells are mostly attributed to clusters 13, 20, 22, 23 and 24 when the front has progressed further inland across Germany. A period of solar heating is likely required after the front passes before convective initiation is favourable. Clusters 22, 23 and 24 also highlight how cold fronts become deformed on their interaction with the Alps (Schumann, 1987). Cluster 17 is worthy of mentioning due to the high cell frequency per timestep near the German-Czech border. These plots provide useful insight for forecasters highlighting where in respect to the front cells are most likely for given front types and their corresponding geographical locations.

3.4 The nature of convective cells

As mentioned in Section 2.2, KONRAD defines a convective cell based on reflectivity and area thresholds. Namely, a convective cell is defined as a cell with 15 pixels (~15 km^2) or more exceeding 46 dBZ. Furthermore, a hail flag value of 1 is assigned if at least one pixel in the cell exceeds 55 dBZ. A hail flag value of 2 is assigned if 12 or more pixels exceed 55 dBZ or if at least one pixel exceeds 60 dBZ. Using the same definitions of cold-frontal and non-cold-frontal cell days as in Figure 3, Figure 9 highlights that mostly all cell days have at least one cell with the hail flag value 1; 96% of cold-frontal cell days and 87% of non-cold-frontal cell days. However, with increasing number of pixels a discrepancy is found. For example, 69% of cold-frontal cell days have a cell with 12 pixels exceeding 55 dBZ (similar criterion for hail flag 2), opposed to only 46% of

https://doi.org/10.5194/nhess-2023-39
Preprint. Discussion started: 28 March 2023


Natural Hazards and Earth System Sciences Discussions

non-cold-frontal cell days. The discrepancy becomes larger for increasing number of pixels. Around 30% of cold-frontal cell days have a cell with 50 pixels exceeding 55 dBZ, opposed to only 10% of non-cold-frontal days. These results highlight that given cells initiate in proximity to a cold front, cells with larger intense cores are more likely to develop. These larger cores could be linked to an increased number of strong convective lines present on cold-frontal cell days. The 55 dBZ threshold has also been proposed as a reflectivity threshold for hail (Mason, 1971). Several studies have evaluated the threshold (e.g., Hohl et al., 2002; Wapler et al., 2012 and Kunz and Kugel, 2015). More recently, Wapler (2017) validated the hail flag against ESWD reports showing that 72% of 2 cm or larger hail reports and 84% of 5 cm or larger hail reports were labelled hail flag 2. Wapler (2017) also found that the synoptic pattern most commonly associated with hail in Germany is a cyclonic south-westerly flow. Such a synoptic pattern is often associated with a cold front. Schemm et al. (2016) found up to 45% of hail events in north-eastern and southern Switzerland formed in pre-frontal zones. They argued that vertical wind shear and along frontal moisture transport were among the mechanisms favouring hail formation in pre-frontal environments. Additionally, Kunz et al. (2020) showed frontal hailstorms produce larger hail and have a longer track on average. Future studies should utilise hail reports such as those collected in the ESWD and automatic front detection on a pan-European scale to better understand the link between cold fronts and hail in Europe.

Figure 10 shows several characteristics of convective cells depending on the cell-front distance. The average for non-cold-frontal cells (dashed green line) is shown for reference. The maximum mean cell lifetime (Figure 10a) of around 20 minutes is found 450–750 km ahead of the 700 hPa front, thus pre-surface-frontal. For the first cell detection the lifetime assigned is 5 minutes and for subsequent timesteps 5 minutes is added. Pre-700-frontal cells further than 150 km from the 700 hPa front have a longer lifetime than the non-cold-frontal 18 minute average. Cells near-700-frontal and post-700-frontal have the shortest lifetime. Due to the convective cell definition of 46 dBZ (15 pixels), the cell lifetime refers to the time a cell exceeds these thresholds rather than the overall lifetime of the cell, thus the actual lifetime of the convection transitioning from the development, mature and decay phase would be longer. Cell splitting and merging can also lead to an unrealistic lifetime in some cases (see section 2.1 of Wapler, 2021).

As shown by Wapler and James (2014) convective cells in Germany propagate in different directions and with different speeds depending on the synoptic pattern. The cell speed is important as it can favour the likelihood of certain convective hazards. Slowly propagating convective systems typically lead to an increased chance of flooding. For example, a series of slowly moving thunderstorms under weak flow led to severe flooding in Germany in 2006 (Piper et al., 2016). On the other hand, faster propagating systems are more likely to be associated with severe convective winds. For example, Gatzen et al. (2020) showed that both warm and cold season bow echoes in Germany occurred under strong 500 hPa flow. In cold-frontal environments we find cells propagate faster than non-cold-frontal cells at all locations relative to the front (Figure 10b). The maximum mean cell speed is found 150–250 km ahead of the 700 hPa front. Two minimums are found, one 550–650 km ahead of the 700 hPa front (pre-surface-frontal) and 650–750 km behind the 700 hPa front.

Once convection has initiated, secondary convection is sometimes found in proximity due to interactions between cell outflows and other boundaries (Wulfmeyer et al., 2011). Radar and satellite observations highlight that post-frontal convective

https://doi.org/10.5194/nhess-2023-39
Preprint. Discussion started: 28 March 2023


Natural Hazards and Earth System Sciences Discussions

cells are typically scattered in nature (Theusner and Hauf, 2004 and Weusthoff and Hauf, 2008). Theusner and Hauf (2004) showed that 72% of post-700-frontal cells were single cells based on 39 warm-season days in Germany. We calculate the number of cells present within a 100 km radius at the detection time to provide an estimate of the aforementioned interactions (Figure 10c). We find that pre-surface-frontal cells (350–750 km) have the largest number of cells present in a 100 km radius (around 4 other cells). Cell outflow boundaries interacting with other surface convergence lines such as the surface front and pre-surface-frontal lines could result in increased convergence and the initiation of new cells. The minimum is found near-700-frontal where only 1 additional cell is present on average. Post-700-frontal cells are also associated with a smaller amount of cells in proximity (1–1.5 cells) compared to pre-700-frontal cells and non-frontal cells (2.25 cells). Analysing such small-scale interactions in observational or model data could be an interesting topic for future studies.

Figure 10d indicates the fraction of cells associated with lightning depending on the cell-front distance. A cell is considered to be associated with lightning if 3 or more lightning strokes are detected 20 km or less from the cell centre during the cell's lifetime. We require at least 3 strokes to filter out any erroneous detected strokes as was carried by Púčik et al. (2015) to confirm presence of a thunderstorm. The lightning fraction maximum is found 550–650 km ahead of the 700 hPa front. Other pre-surface-frontal cells are also commonly associated with lightning (around 80% of cells). The fraction of cells associated with lightning sharply declines with increasing proximity to the 700 hPa cold front. The fraction of cells with lightning increases again in the post-700-frontal environment but the overall fraction with lightning is lower than most pre-700-frontal cells and the non-frontal fraction (0.73). Observational studies have indicated that low instability in the lower mixed-phase region can discriminate between convection associated with lightning and non-lightning convection (e.g., van den Broeke et al., 2005). Differences in the typical vertical profile could vary across the front explaining the observed differences in lightning probability.

Figure 10e is complementary to Figure 9 highlighting it is generally pre-surface-frontal cells that have an increased likelihood of becoming intense compared to non-cold-frontal cells. Like the cell lifetime, cells further than 150 km ahead of the 700 hPa front surpass the non-cold-frontal average. The largest fraction with the hail flag (around 12%) is cells 550–650 km ahead of the 700 hPa front, around 200 km ahead of the cell frequency maximum (Figure 4). As with the lightning fraction, near-700-frontal cells have the lowest fraction associated with the hail flag 2. Following the result that near-700-frontal cells are typically less intense one may suspect the lower lightning fraction is simply related to cell intensity. However, upon considering cells that only meet the minimum cell threshold (15 pixels at 46 dBZ and no pixels at 55 dBZ), the same distribution was found with the lowest lightning fraction near-700-frontal and the largest pre-surface-frontal. The largest post-700-frontal hail flag 2 fraction is found between 250–450 km behind the 700 hPa front which corresponds closely to the post-700-frontal cell frequency maximum (Figure 4).

Mesoyclones, where a rotating updraft is present, are known to be linked to severe convective hazards such as hail and tornadoes. Wapler (2017) showed 75% of hail events in Germany were associated with mesocyclones. Based on the mesocyclone criteria introduced in section 2.2 we find that around 1.5% of non-cold-frontal cells are associated with mesocyclones. However, the fraction of pre-surface-frontal cells is three times the non-cold-frontal fraction. Near-700-frontal cells are also more likely to be associated with a mesocyclone than non-cold-frontal or post-700-frontal cells. A key result from this section is that while convective cells are most frequent near the surface front, when they do develop further ahead of the surface front they

https://doi.org/10.5194/nhess-2023-39
Preprint. Discussion started: 28 March 2023


Natural Hazards and Earth System Sciences Discussions

are more likely to be associated with lightning, intense cores and mesocyclones, especially in comparison to non-cold-frontal cells.

4 Conclusion

A novel climatology of cold-frontal convective cells in Germany (and surrounding areas) has been produced using automatic front detection methods and a convective cell detection and tracking dataset during the warm-season from 2007–2016. Furthermore, the nature of cells such as lightning activity, cell propagation speed and intensity has been analysed. Previous cold-frontal convection studies in Europe had primarily focused on narrow cold-frontal rainbands (Gatzen, 2011 and Clark, 2013) or on cold-frontal hailstorms (Schemm et al., 2016 and Kunz et al., 2020). In this study, we focused on the nature and climatological differences of convective cells depending on their distance from the front as well as making a comparison with non-cold-frontal cells.

The primary findings of the study are outlined below:

- Cold-frontal cell days are associated with around twice as many cells on average compared to non-cold-frontal cell days. Convection is likely to be more widespread across Germany on cold-frontal cell days and linked to more cells per cluster. Cold-frontal cell days are more likely to be associated with convective cells with large intense cores. Around 30% of cold-frontal convective cell days were associated with at least one cell with a 50 km^2 area exceeding 55 dBZ opposed to only 10% of non-cold-frontal cell days.
- Convective cells are most frequent 350–400 km ahead of the 700 hPa frontal line, which is marginally ahead of the mean surface front location. The minimum cell frequency is directly at the 700 hPa front with over 5 times less cells developing near-700-frontal compared to the 350–400 km maximum. Post-700-frontal cells most commonly develop 350–400km behind the 700 hPa front.
- Post-700-frontal and non-cold-frontal cells exhibit a typical convective diurnal cycle with a maximum between 15–16 UTC. Pre-700-frontal cells however exhibit a weakened diurnal cycle with around a third of all cells developing between 21–06 UTC. The weakened cycle is consistent with observations of mesoscale convective systems and mesocyclones in Europe.
- Post-700-frontal cells are most frequent in north-west Germany, particularly close to the coast. Pre-700-frontal and non-cold-frontal cells show similar spatial distributions with cells most frequent in the southern half of Germany. Cells in south-east and eastern Germany are less associated with cold fronts than other regions. Cold-frontal cell frequencies are highest in Germany when a front is orientated NE-SW to the west or north-west of Germany.
- Pre-700-frontal cells (particularly pre-surface-frontal cells) were found to be longer-living, more often associated with intense cores, and with more lightning and mesocyclones than cells in other categories. The opposite is true for post-

https://doi.org/10.5194/nhess-2023-39
Preprint. Discussion started: 28 March 2023


Natural Hazards and Earth System Sciences Discussions

700-frontal cells compared to the non-cold-frontal cells excluding mesocyclones where less significant differences were found between the non-cold-frontal and post-700-frontal fractions. Cells at all distances relative to the front propagate faster on average than non-cold-frontal cells.

These results act as an important reference for future studies on cold-frontal convection. Since our results have shown the climatology and nature of convective cells vary substantially in Germany depending on their cell-front distance and in comparison to non-cold-frontal cells, this research should prompt further studies on cold-frontal convection especially regarding links to convective hazards. Future studies should also be performed on a pan-European scale to highlight any potential spatial differences in cold-frontal convection climatology.

Code and data availability. ERA5 data can be downloaded from the Copernicus servers (ERA5). KONRAD is available for research purposes on request (contact kundenservice@dwd.de). Front detection and plotting code are available on request from the corresponding author.

Author contributions. SP and LS wrote the original research proposal. GP carried out the data analysis and wrote all sections of the manuscript. SP, LS and KW provided comments and support during the data analysis and manuscript process. KW provided technical support with the KONRAD cell detection and tracking dataset.

Competing interests. The authors declare there are no competing interests

Acknowledgements. This research has been funded by Deutsche Forschungsgemeinschaft (DFG) through grant CRC 1114 'Scaling Cascades in Complex Systems, Project Number 235221301', Project C06 "Multi-scale structure of atmospheric vortices". We thank Stefan Rüdisühli for useful discussions and insight regarding front detection methods.

Name	Cold-frontal cell days	Non-cold-frontal cell days	All cell days
Cell Count	163,255	94,963	258,218
Days	614	775	1,389
Cells per day	265.9	122.5	185.9

Table 1. Summary of convective cell datasets. A cold-frontal cell day is defined as one where at least one convective cell was detected within 750 km of the 700 hPa cold-frontal line, otherwise the day is classified as a non-cold-frontal cell day.

https://doi.org/10.5194/nhess-2023-39
Preprint. Discussion started: 28 March 2023

Natural Hazards and Earth System Sciences
Discussions
Open Access
EGU

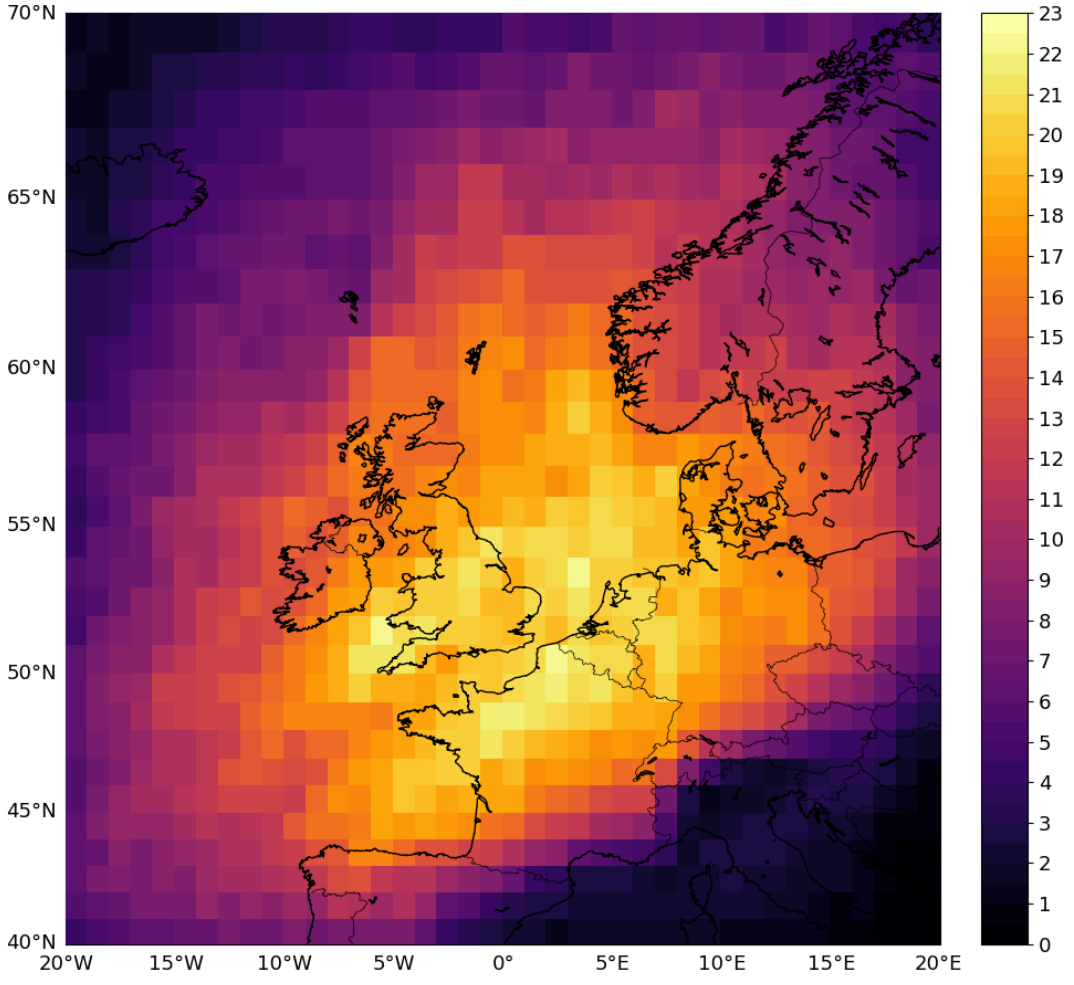

Figure 1. Number of cold-frontal days per warm-season between 2007–2016 for 1 x 1 degree grid boxes in the domain [40N-70N, 20W–20E].

https://doi.org/10.5194/nhess-2023-39
Preprint. Discussion started: 28 March 2023

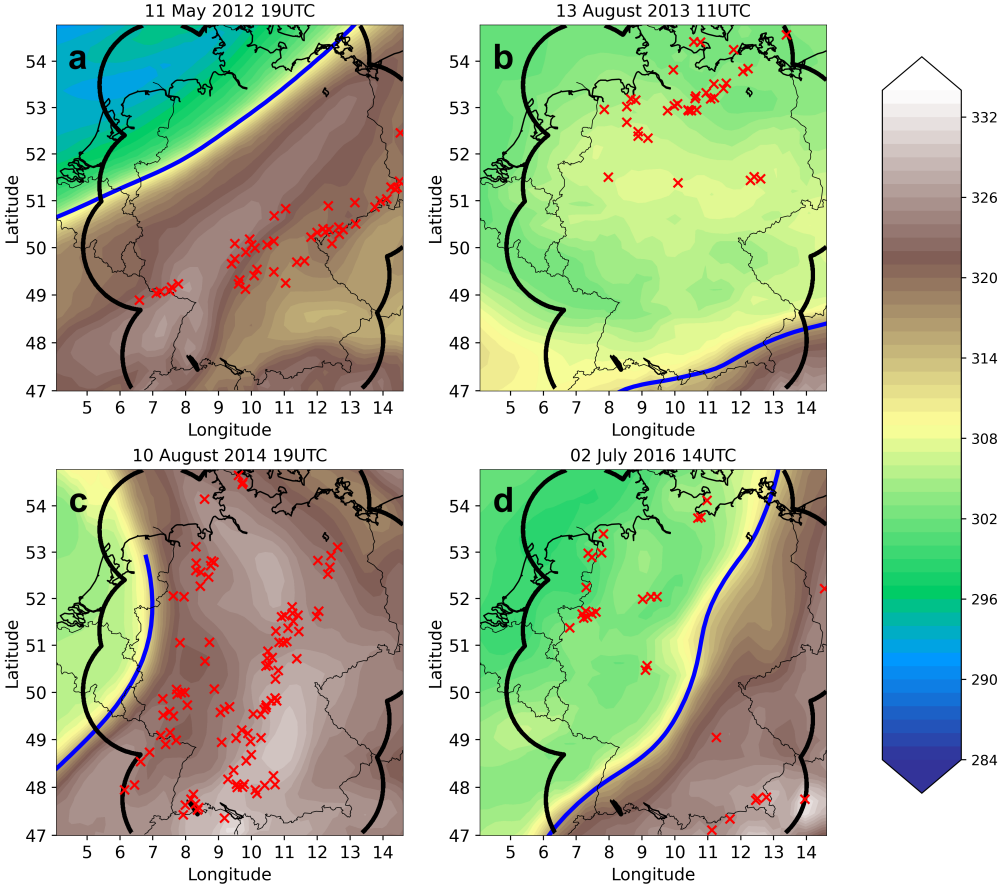

Figure 2. 700 hPa cold-frontal line (blue), convective cells (red crosses) and 700 hPa equivalent potential temperature in kelvin (shaded) for four cases at single timesteps. The black contour shows the KONRAD convective cell domain.

https://doi.org/10.5194/nhess-2023-39
Preprint. Discussion started: 28 March 2023

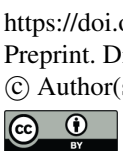

Natural Hazards and Earth System Sciences
Discussions
Open Access
EGU

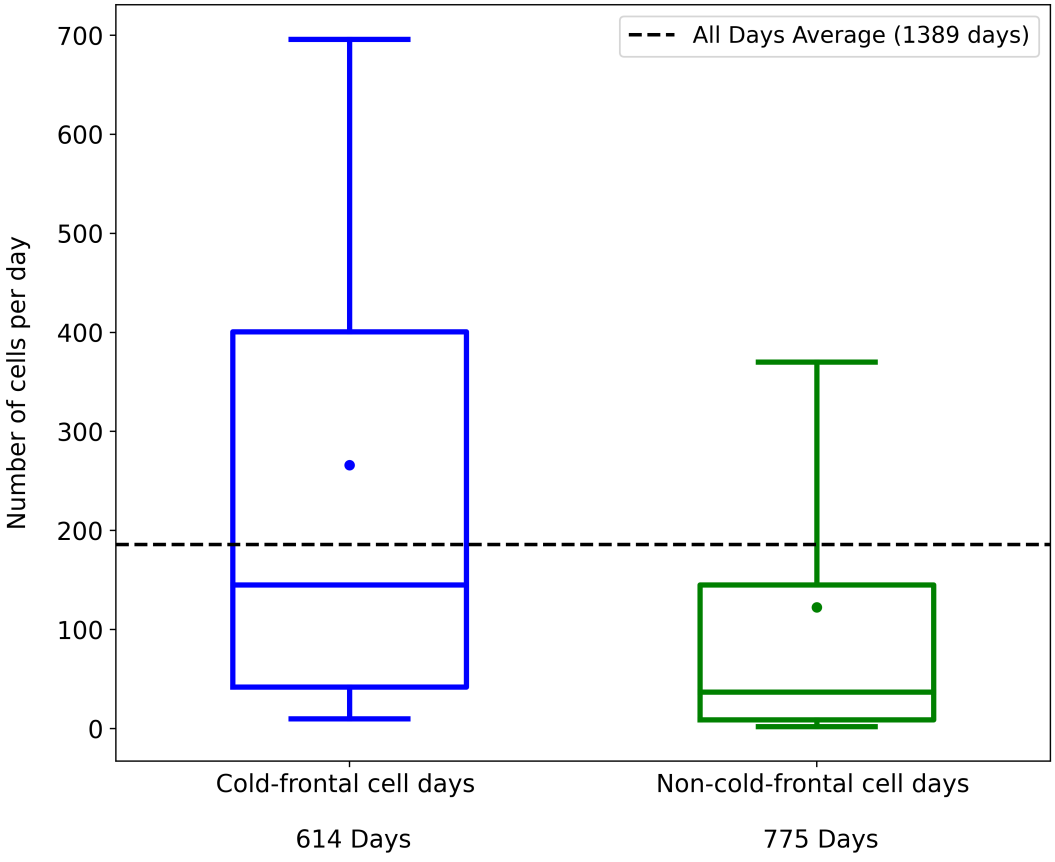

Figure 3. Number of cells per day boxplots for cold-frontal cell days and non-cold-frontal cell days. A cold-frontal cell day is defined as one where at least one convective cell was detected within 750 km of the 700 hPa frontal line, otherwise the day is classified as a non-cold-frontal cell day. The median is represented as a horizontal line, dots represent the mean, boxes represent the 25th–75th percentile values, and whiskers represent the 10th and 90th percentile values. The all days mean (1389 days) is shown by the dashed black line.

https://doi.org/10.5194/nhess-2023-39
Preprint. Discussion started: 28 March 2023

Natural Hazards and Earth System Sciences
Discussions
Open Access
EGU

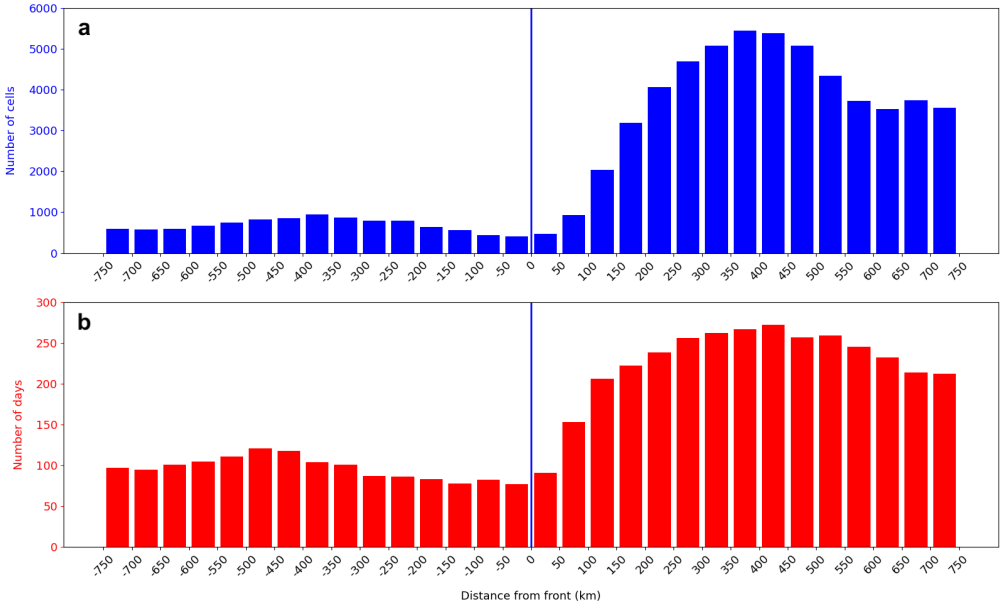

Figure 4. Number of convective cells (a) and number of convective cell days (b) depending on the cell-front distance. Positive and negative distances represent the pre-700-frontal and post-700-frontal environments, respectively.

https://doi.org/10.5194/nhess-2023-39
Preprint. Discussion started: 28 March 2023

Natural Hazards and Earth System Sciences
Discussions
Open Access
EGU

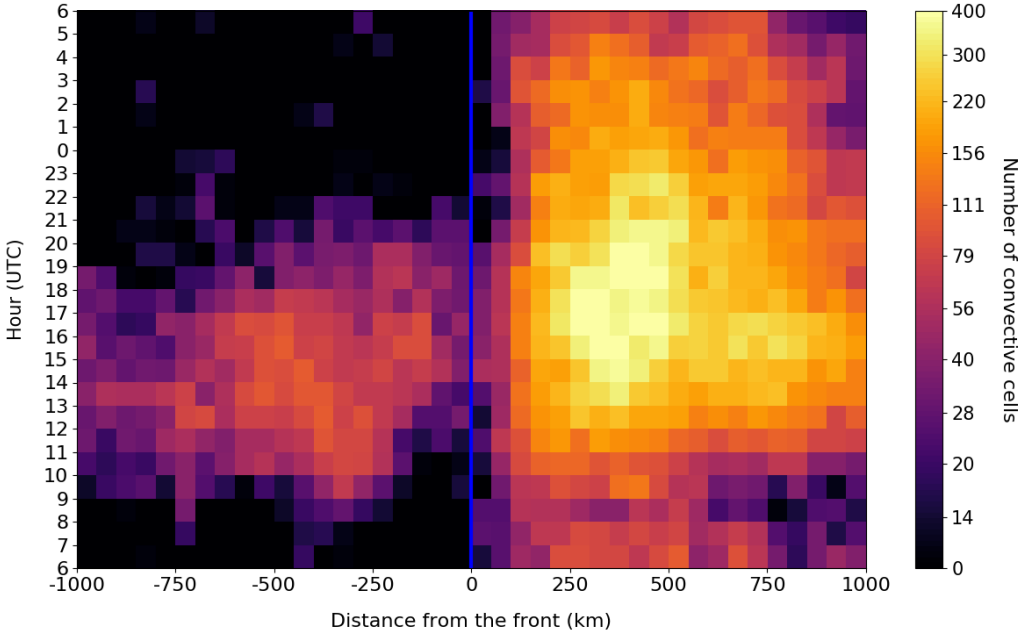

Figure 5. Number of convective cells (colours) depending on the cell-front distance (horizontal axis) and hour of the day (vertical axis). Negative distances indicate post-700-frontal cells while positive distances indicate pre-700-frontal cells.

https://doi.org/10.5194/nhess-2023-39
Preprint. Discussion started: 28 March 2023

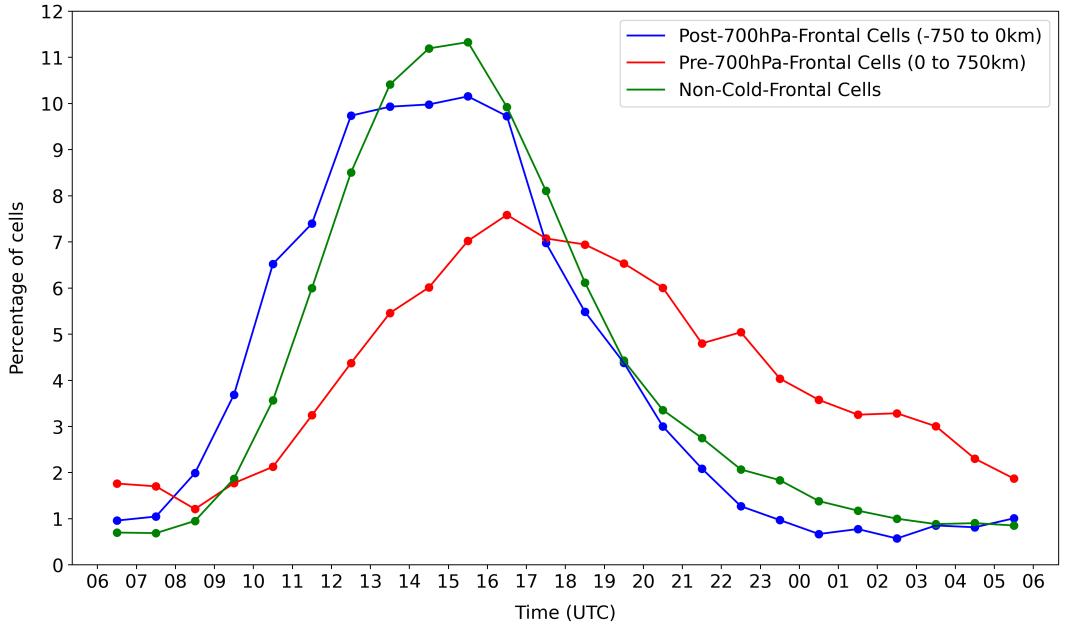

Figure 6. Diurnal cycle of convective cells for post-700-frontal (blue), pre-700-frontal (red) and non-cold-frontal cells (green).

https://doi.org/10.5194/nhess-2023-39
Preprint. Discussion started: 28 March 2023

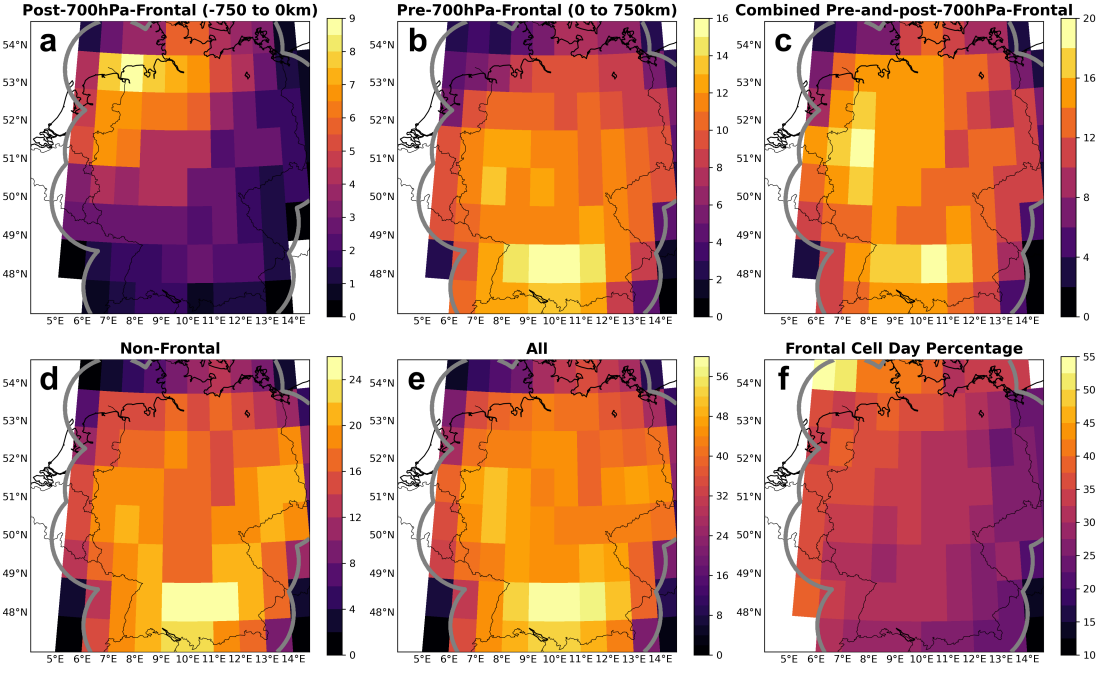

Figure 7. Number of convective cell days per warm season for 1 x 1 degree grid boxes for post-700-frontal cells (a), pre-700-frontal cells (b), cold-frontal cells (c), non-cold-frontal cells (d), all cells (e). Panel f shows the percentage of convective cell days associated with cold fronts (panel c divided by panel e). Note the different colourbar levels.

https://doi.org/10.5194/nhess-2023-39
Preprint. Discussion started: 28 March 2023

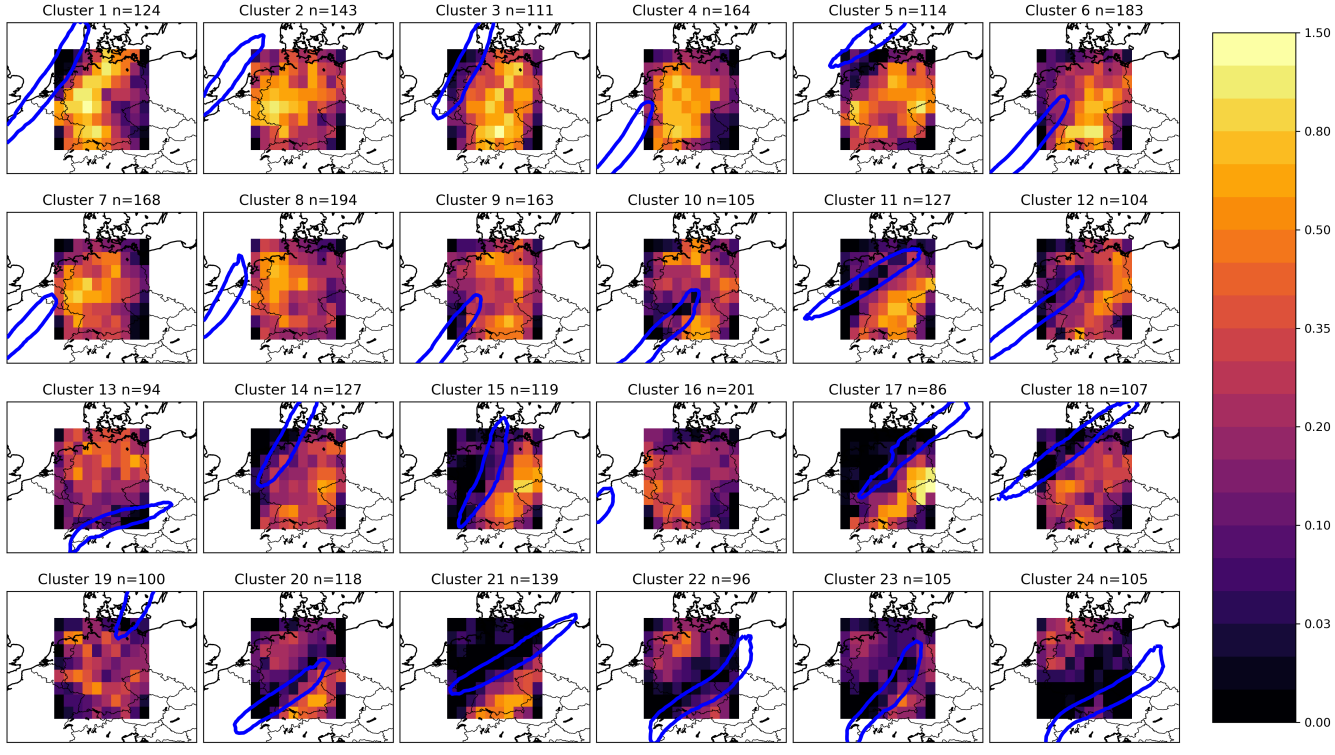

Figure 8. Clustered fronts using the k-means clustering algorithm in the domain [40N–60N,0–20E]. Subplot header represents the number of timesteps (n) contained in each cluster. The colourbar represents the number of convective cells per 1 x 1 degree grid box per timestep. The blue contours indicate where 50% of timesteps in the respective cluster have the front located at that grid point.

https://doi.org/10.5194/nhess-2023-39
Preprint. Discussion started: 28 March 2023

Natural Hazards and Earth System Sciences
Discussions

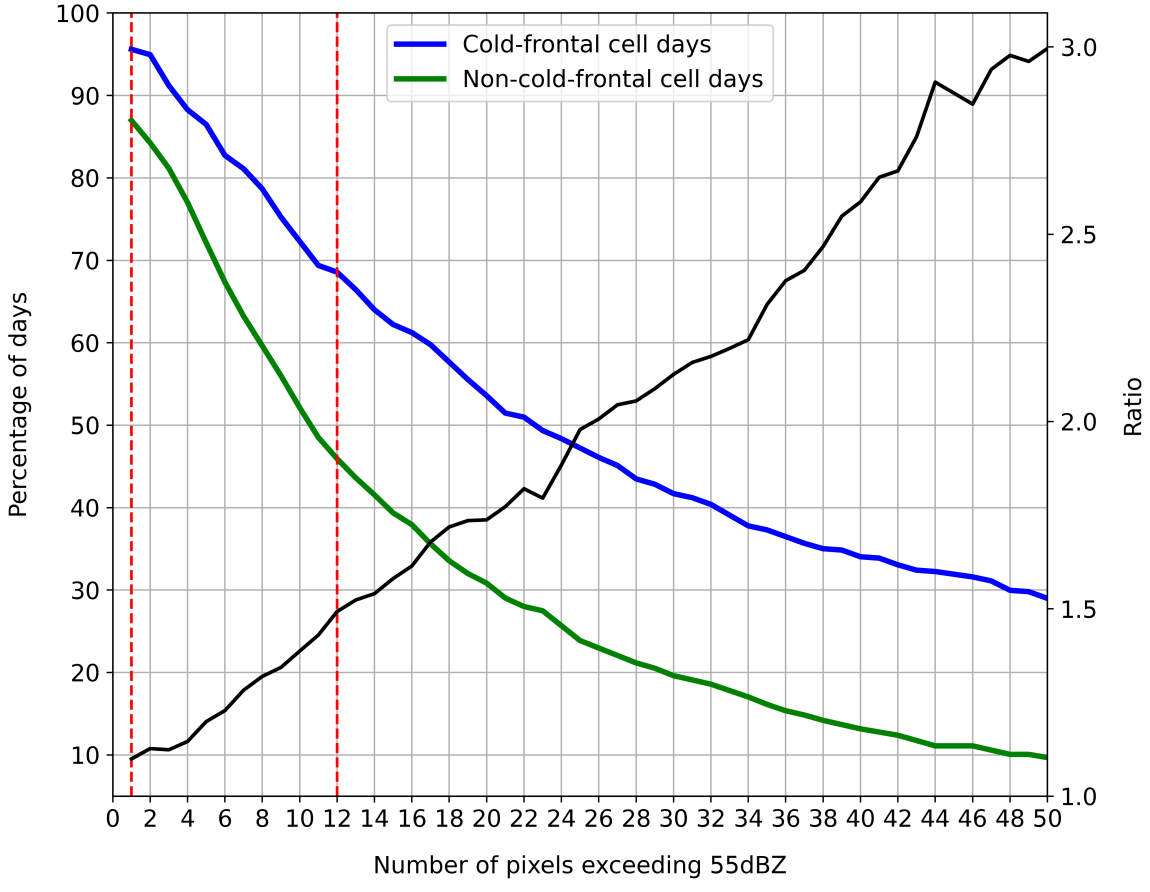

Figure 9. Percentage of days with at least one cell with n pixels exceeding 55 dBZ for cold-frontal cell days (blue) and non-cold-frontal cell days (green). The ratio (black) of frontal to non-cold-frontal cell days is shown on the secondary axis. The first dashed red line represents the hail flag 1 and second dashed line represents the hail flag 2 (excluding the 1 pixel exceeding 60 dBZ criterion).

https://doi.org/10.5194/nhess-2023-39
Preprint. Discussion started: 28 March 2023

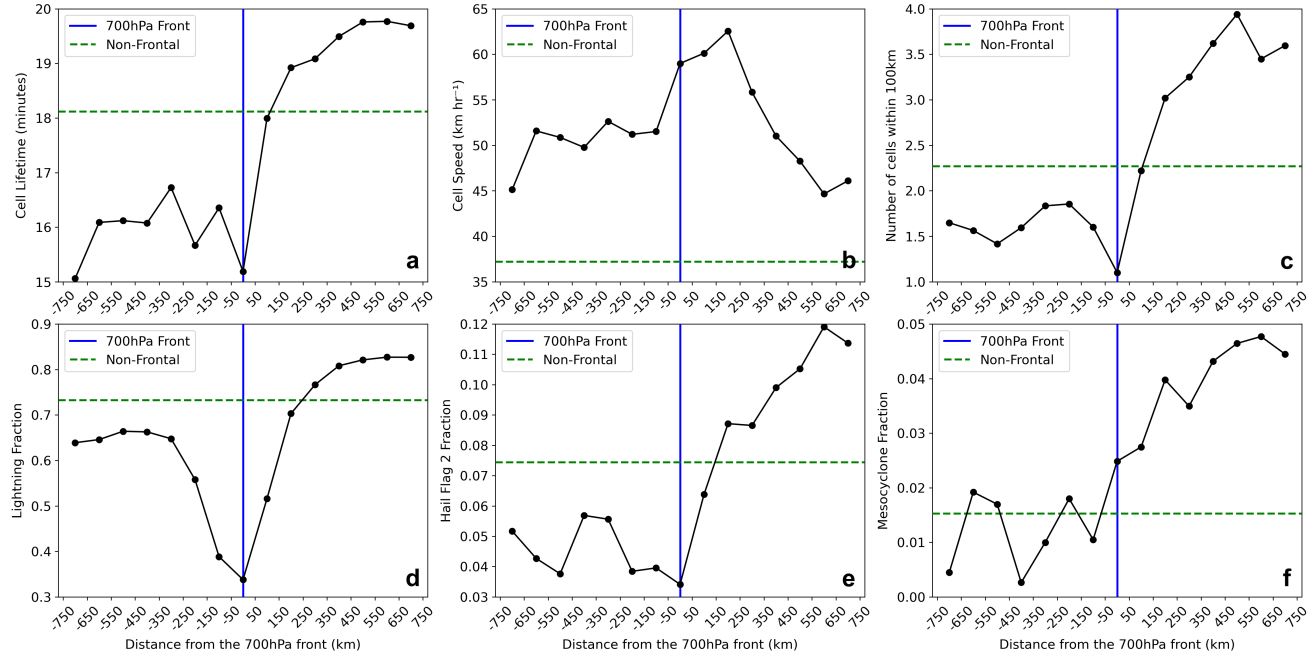

Figure 10. Mean cell lifetime (a), mean cell speed (b), mean number of cells within 100 km of cell centre (c), fraction of cells with lightning (d), fraction with hail flag 2 (e) and fraction with mesocyclones (f) depending on the cell-front distance (km). The dashed green line represents the non-cold-frontal cells fraction for reference.

https://doi.org/10.5194/nhess-2023-39
Preprint. Discussion started: 28 March 2023

References

Ban, N., Schmidli, J., and Schär, C.: Evaluation of the convection-resolving regional climate modeling approach in decade-long simulations, Journal of Geophysical Research: Atmospheres, 119, 7889–7907, https://doi.org/10.1002/2014JD021478, 2014.

Betz, H. D., Schmidt, K., Laroche, P., Blanchet, P., Oettinger, W. P., Defer, E., Dziewit, Z., and Konarski, J.: Linet—an international lightning detection network in Europe, Atmospheric Research, 91, 564–573, https://doi.org/10.1016/j.atmosres.2008.06.012, 2009.

Bluestein, H. B.: Synoptic-dynamic meteorology in midlatitudes. Volume II. Observations and theory of weather systems, Oxford University Press, https://www.osti.gov/biblio/6227041, 1993.

Bott, A.: Synoptische Meteorologie, Springer Berlin, Heidelberg, 2nd edn., 2012.

Catto, J. L. and Pfahl, S.: The importance of fronts for extreme precipitation, Journal of Geophysical Research: Atmospheres, 118, 10,791–10,801, https://doi.org/10.1002/jgrd.50852, 2013.

Clark, M.: A provisional climatology of cool-season convective lines in the UK, Atmospheric Research, 123, 180–196, https://doi.org/10.1016/j.atmosres.2012.09.018, 6th European Conference on Severe Storms 2011. Palma de Mallorca, Spain, 2013.

Dahl, J. M. L. and Fischer, J.: The Origin of Western European Warm-Season Prefrontal Convergence Lines, Weather and Forecasting, 31, 1417 – 1431, https://doi.org/10.1175/WAF-D-15-0161.1, 2016.

Davies, H. and Wernli, H.: DYNAMICAL METEOROLOGY | Quasigeostrophic Theory, in: Encyclopedia of Atmospheric Sciences (Second Edition), edited by North, G. R., Pyle, J., and Zhang, F., pp. 393–403, Academic Press, Oxford, second edition edn., https://doi.org/10.1016/B978-0-12-382225-3.00326-1, 2015.

Dotzek, N., Groenemeijer, P., Feuerstein, B., and Holzer, A.: Overview of ESSL's severe convective storms research using the European Severe Weather Database ESWD, Atmos. Res., 93, 575–586, 2009.

ERA5: https://cds.climate.copernicus.eu/cdsapp!/search?text=ERA5 (Accessed March 2023).

Ferretti, R., Pichelli, E., Gentile, S., Maiello, I., Cimini, D., Davolio, S., Miglietta, M. M., Panegrossi, G., Baldini, L., Pasi, F., Marzano, F. S., Zinzi, A., Mariani, S., Casaioli, M., Bartolini, G., Loglisci, N., Montani, A., Marsigli, C., Manzato, A., Pucillo, A., Ferrario, M. E., Colaiuda, V., and Rotunno, R.: Overview of the first HyMeX Special Observation Period over Italy: observations and model results, Hydrology and Earth System Sciences, 18, 1953–1977, https://doi.org/10.5194/hess-18-1953-2014, 2014.

Gatzen, C.: A 10-year climatology of cold-season narrow cold-frontal rainbands in Germany, Atmospheric Research, 100, 366–370, https://doi.org/10.1016/j.atmosres.2010.09.018, 5th European Conference on Severe Storms, 2011.

Gatzen, C. P., Fink, A. H., Schultz, D. M., and Pinto, J. G.: An 18-year climatology of derechos in Germany, Natural Hazards and Earth System Sciences, 20, 1335–1351, https://doi.org/10.5194/nhess-20-1335-2020, 2020.

Groenemeijer, P., Púčik, T., Holzer, A. M., Antonescu, B., Riemann-Campe, K., Schultz, D. M., Kühne, T., Feuerstein, B., Brooks, H. E., Doswell, C. A., Koppert, H.-J., and Sausen, R.: Severe Convective Storms in Europe: Ten Years of Research and Education at the European Severe Storms Laboratory, Bulletin of the American Meteorological Society, 98, 2641 – 2651, https://doi.org/10.1175/BAMS-D-16-0067.1, 2017.

Hengstebeck, T., Wapler, K., Heizenreder, D., and Joe, P.: Radar Network–Based Detection of Mesocyclones at the German Weather Service, Journal of Atmospheric and Oceanic Technology, 35, 299 – 321, https://doi.org/10.1175/JTECH-D-16-0230.1, 2018.

Hersbach, H., Bell, B., Berrisford, P., Biavati, G., Horányi, A., Muñoz Sabater, J., Nicolas, J., Peubey, C., Radu, R., Rozum, I., Schepers, D., Simmons, A., Soci, C., Dee, D., and Thépaut, J.-N.: ERA5 hourly data on pressure levels from 1959 to present, Copernicus Climate Change Service (C3S) Climate Data Store (CDS). (Accessed on 08–JAN-2021), https://doi.org/10.24381/cds.bd0915c6, 2018.

https://doi.org/10.5194/nhess-2023-39
Preprint. Discussion started: 28 March 2023

Hersbach, H., Bell, B., Berrisford, P., Hirahara, S., Horányi, A., Muñoz-Sabater, J., Nicolas, J., Peubey, C., Radu, R., Schepers, D., Simmons, A., Soci, C., Abdalla, S., Abellan, X., Balsamo, G., Bechtold, P., Biavati, G., Bidlot, J., Bonavita, M., De Chiara, G., Dahlgren, P., Dee, D., Diamantakis, M., Dragani, R., Flemming, J., Forbes, R., Fuentes, M., Geer, A., Haimberger, L., Healy, S., Hogan, R. J., Hólm, E., Janisková, M., Keeley, S., Laloyaux, P., Lopez, P., Lupu, C., Radnoti, G., de Rosnay, P., Rozum, I., Vamborg, F., Villaume, S., and Thépaut, J.-N.: The ERA5 global reanalysis, Quarterly Journal of the Royal Meteorological Society, 146, 1999–2049, https://doi.org/10.1002/qj.3803, 2020.

Hewson, T. D.: Objective fronts, Meteorological Applications, 5, 37–65, https://doi.org/10.1017/S1350482798000553, 1998.

Hoeppe, P.: Trends in weather related disasters – Consequences for insurers and society, Weather and Climate Extremes, 11, 70–79, https://doi.org/10.1016/j.wace.2015.10.002, observed and Projected (Longer-term) Changes in Weather and Climate Extremes, 2016.

Hohl, R., Schiesser, H.-H., and Aller, D.: Hailfall: the relationship between radar-derived hail kinetic energy and hail damage to buildings, Atmospheric Research, 63, 177–207, https://doi.org/10.1016/S0169-8095(02)00059-5, 2002.

Jenkner, J., Sprenger, M., Schwenk, I., Schwierz, C., Dierer, S., and Leuenberger, D.: Detection and climatology of fronts in a high-resolution model reanalysis over the Alps, Meteorological Applications, 17, 1–18, https://doi.org/10.1002/met.142, 2010.

Karney, C. F. F.: Algorithms for geodesics, Journal of Geodesy, 87, 43–55, https://doi.org/10.1007/s00190-012-0578-z, 2013.

Kunz, M. and Kugel, P. I.: Detection of hail signatures from single-polarization C-band radar reflectivity, Atmospheric Research, 153, 565–577, https://doi.org/10.1016/j.atmosres.2014.09.010, 2015.

Kunz, M., Blahak, U., Handwerker, J., Schmidberger, M., Punge, H. J., Mohr, S., Fluck, E., and Bedka, K. M.: The severe hailstorm in southwest Germany on 28 July 2013: characteristics, impacts and meteorological conditions, Quarterly Journal of the Royal Meteorological Society, 144, 231–250, https://doi.org/10.1002/qj.3197, 2018.

Kunz, M., Wandel, J., Fluck, E., Baumstark, S., Mohr, S., and Schemm, S.: Ambient conditions prevailing during hail events in central Europe, Natural Hazards and Earth System Sciences, 20, 1867–1887, https://doi.org/10.5194/nhess-20-1867-2020, 2020.

Lee, K.-O., Flamant, C., Ducrocq, V., Duffourg, F., Fourrié, N., and Davolio, S.: Convective initiation and maintenance processes of two back-building mesoscale convective systems leading to heavy precipitation events in Southern Italy during HyMeX IOP 13, Quarterly Journal of the Royal Meteorological Society, 142, 2623–2635, https://doi.org/10.1002/qj.2851, 2016.

Markowski, P. and Richardson, Y.: Mesoscale Meteorology in Midlatitudes, vol. 2 of *Advancing weather and climate science*, Wiley, Somerset, 1. aufl. edn., 2010.

Mason, B. J.: THE PHYSICS OF CLOUDS. 2ND ED, CLARENDON PR, 1971.

Mohr, S., Ehret, U., Kunz, M., Ludwig, P., Caldas-Alvarez, A., Daniell, J. E., Ehmele, F., Feldmann, H., Franca, M. J., Gattke, C., Hundhausen, M., Knippertz, P., Küpfer, K., Mühr, B., Pinto, J. G., Quinting, J., Schäfer, A. M., Scheibel, M., Seidel, F., and Wisotzky, C.: A multi-disciplinary analysis of the exceptional flood event of July 2021 in central Europe – Part 1: Event description and analysis, Natural Hazards and Earth System Sciences, 23, 525–551, https://doi.org/10.5194/nhess-23-525-2023, 2023.

Morel, C. and Senesi, S.: A climatology of mesoscale convective systems over Europe using satellite infrared imagery. II: Characteristics of European mesoscale convective systems, Quarterly Journal of the Royal Meteorological Society, 128, 1973–1995, https://doi.org/10.1256/003590002320603494, 2002.

Piper, D., Kunz, M., Ehmele, F., Mohr, S., Mühr, B., Kron, A., and Daniell, J.: Exceptional sequence of severe thunderstorms and related flash floods in May and June 2016 in Germany – Part 1:
Meteorological background, Natural Hazards and Earth System Sciences, 16, 2835–2850, https://doi.org/10.5194/nhess-16-2835-2016, 2016.

https://doi.org/10.5194/nhess-2023-39
Preprint. Discussion started: 28 March 2023

Púčik, T., Groenemeijer, P., Rýva, D., and Kolář, M.: Proximity Soundings of Severe and Nonsevere Thunderstorms in Central Europe, Monthly Weather Review, 143, 4805 – 4821, https://doi.org/10.1175/MWR-D-15-0104.1, 2015.

Renard, R. J. and Clarke, L.: EXPERIMENTS IN NUMERICAL OBJECTIVE FRONTAL ANALYSIS1, Monthly Weather Review, 93, 547–556, 1965.

Rüdisühli, S., Sprenger, M., Leutwyler, D., Schär, C., and Wernli, H.: Attribution of precipitation to cyclones and fronts over Europe in a kilometer-scale regional climate simulation, Weather and Climate Dynamics, 1, 675–699, 2020.

Schemm, S., Rudeva, I., and Simmonds, I.: Extratropical fronts in the lower troposphere–global perspectives obtained from two automated methods, Quarterly Journal of the Royal Meteorological Society, 141, 1686–1698, https://doi.org/10.1002/qj.2471, 2015.

Schemm, S., Nisi, L., Martinov, A., Leuenberger, D., and Martius, O.: On the link between cold fronts and hail in Switzerland, Atmospheric Science Letters, 17, 315–325, 2016.

Schemm, S., Sprenger, M., and Wernli, H.: When during Their Life Cycle Are Extratropical Cyclones Attended by Fronts?, Bulletin of the American Meteorological Society, 99, 149 – 165, https://doi.org/10.1175/BAMS-D-16-0261.1, 2018.

Schumacher, R. S., Childs, S. J., and Adams-Selin, R. D.: Intense Surface Winds from Gravity Wave Breaking in Simulations of a Destructive Macroburst, Monthly Weather Review, https://doi.org/10.1175/MWR-D-22-0103.1, 2022.

Schumann, U.: Influence of Mesoscale Orography on Idealized Cold Fronts, Journal of Atmospheric Sciences, 44, 3423 – 3441, https://doi.org/10.1175/1520-0469(1987)044<3423:IOMOOI>2.0.CO;2, 1987.

Surowiecki, A. and Taszarek, M.: A 10-Year Radar-Based Climatology of Mesoscale Convective System Archetypes and Derechos in Poland, Monthly Weather Review, 148, 3471 – 3488, https://doi.org/10.1175/MWR-D-19-0412.1, 2020.

Taszarek, M., Allen, J., Púčik, T., Groenemeijer, P., Czernecki, B., Kolendowicz, L., Lagouvardos, K., Kotroni, V., and Schulz, W.: A Climatology of Thunderstorms across Europe from a Synthesis of Multiple Data Sources, Journal of Climate, 32, 1813 – 1837, https://doi.org/10.1175/JCLI-D-18-0372.1, 2019.

Taszarek, M., Allen, J. T., Groenemeijer, P., Edwards, R., Brooks, H. E., Chmielewski, V., and Enno, S.-E.: Severe Convective Storms across Europe and the United States. Part I: Climatology of Lightning, Large Hail, Severe Wind, and Tornadoes, Journal of Climate, 33, 10 239 – 10 261, https://doi.org/10.1175/JCLI-D-20-0345.1, 2020.

Theusner, M. and Hauf, T.: A study on the small scale precipitation structure over Germany using the radar network of the German Weather Service, Meteorologische Zeitschrift, 13, 311–322, https://doi.org/10.1127/0941-2948/2004/0013-0311, 2004.

Thomas, C. M. and Schultz, D. M.: What are the Best Thermodynamic Quantity and Function to Define a Front in Gridded Model Output?, Bulletin of the American Meteorological Society, 100, 873 – 895, https://doi.org/10.1175/BAMS-D-18-0137.1, 2019.

van den Broeke, M. S., Schultz, D. M., Johns, R. H., Evans, J. S., and Hales, J. E.: Cloud-to-Ground Lightning Production in Strongly Forced, Low-Instability Convective Lines Associated with Damaging Wind, Weather and Forecasting, 20, 517 – 530, https://doi.org/10.1175/WAF876.1, 2005.

Wapler, K.: The life-cycle of hailstorms: Lightning, radar reflectivity and rotation characteristics, Atmospheric Research, 193, 60–72, https://doi.org/10.1016/j.atmosres.2017.04.009, 2017.

Wapler, K.: Mesocyclonic and non-mesocyclonic convective storms in Germany: Storm characteristics and life-cycle, Atmospheric Research, 248, 105 186, https://doi.org/10.1016/j.atmosres.2020.105186, 2021.

Wapler, K. and James, P.: Thunderstorm occurrence and characteristics in Central Europe under different synoptic conditions, Atmospheric Research, 158, https://doi.org/10.1016/j.atmosres.2014.07.011, 2014.

https://doi.org/10.5194/nhess-2023-39
Preprint. Discussion started: 28 March 2023

Wapler, K., Goeber, M., and Trepte, S.: Comparative verification of different nowcasting systems to support optimisation of thunderstorm warnings, Advances in Science and Research, 8, 121–127, https://doi.org/10.5194/asr-8-121-2012, 2012.

Wapler, K., Hengstebeck, T., and Groenemeijer, P.: Mesocyclones in Central Europe as seen by radar, Atmospheric Research, 168, 112–120, https://doi.org/10.1016/j.atmosres.2015.08.023, 2016.

Werner, M.: KONRAD3D: A new tool for detection and nowcasting of convective cells at DWD, Second European Nowcasting Conference, Offenbach, Germany, http://eumetnet.eu/wp-content/uploads/2017/07/enc_book_of_abstract.pdf, 2017.

Weusthoff, T. and Hauf, T.: The life cycle of convective-shower cells under post-frontal condition, Quarterly Journal of the Royal Meteorological Society, 134, 841–857, https://doi.org/10.1002/qj.260, 2008.

Wilhelm, J., Mohr, S., Punge, H. J., Mühr, B., Schmidberger, M., Daniell, J. E., Bedka, K. M., and Kunz, M.: Severe thunderstorms with large hail across Germany in June 2019, Weather, 76, 228–237, https://doi.org/10.1002/wea.3886, 2021.

Wilks, D. S.: Statistical methods in the atmospheric sciences, International Geophysics Series, 2nd edn., 2006.

Wulfmeyer, V., Behrendt, A., Kottmeier, C., Corsmeier, U., Barthlott, C., Craig, G. C., Hagen, M., Althausen, D., Aoshima, F., Arpagaus, M., Bauer, H.-S., Bennett, L., Blyth, A., Brandau, C., Champollion, C., Crewell, S., Dick, G., Di Girolamo, P., Dorninger, M., Dufournet, Y., Eigenmann, R., Engelmann, R., Flamant, C., Foken, T., Gorgas, T., Grzeschik, M., Handwerker, J., Hauck, C., Höller, H., Junkermann, W., Kalthoff, N., Kiemle, C., Klink, S., König, M., Krauss, L., Long, C. N., Madonna, F., Mobbs, S., Neininger, B., Pal, S., Peters, G., Pigeon, G., Richard, E., Rotach, M. W., Russchenberg, H., Schwitalla, T., Smith, V., Steinacker, R., Trentmann, J., Turner, D. D., van Baelen, J., Vogt, S., Volkert, H., Weckwerth, T., Wernli, H., Wieser, A., and Wirth, M.: The Convective and Orographically-induced Precipitation Study (COPS): the scientific strategy, the field phase, and research highlights, Quarterly Journal of the Royal Meteorological Society, 137, 3–30, https://doi.org/10.1002/qj.752, 2011.